

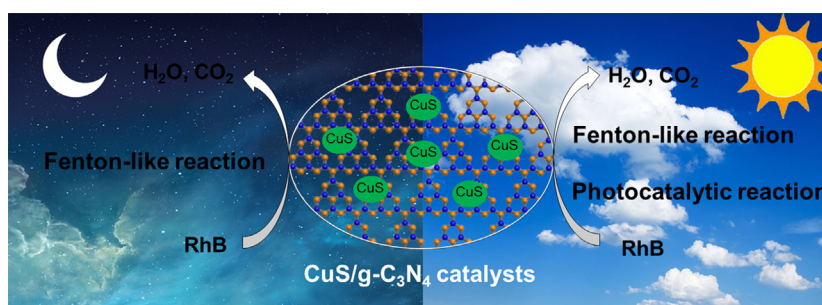
Original Article

Concerted catalytic and photocatalytic degradation of organic pollutants over CuS/g-C₃N₄ catalysts under light and dark conditionsYouliang Ma^{a,b}, Jing Zhang^b, Yun Wang^{a,*}, Qiong Chen^b, Zhongmin Feng^a, Ting Sun^{a,*}^a College of Sciences, Northeastern University, Shenyang 110004, China^b School of Humanities and Sciences, Ningxia Institute of Science and Technology, Shizuishan 753000, China

HIGHLIGHTS

- CuS/g-C₃N₄ composite catalysts were successfully fabricated.
- The optimal mass ratio of CuS in the composite was determined.
- Fenton-like catalytic and photocatalytic effects were combined for sewage purification.
- The continuous degradation of organic pollutants was achieved.

GRAPHICAL ABSTRACT



ARTICLE INFO

Article history:

Received 6 July 2018

Revised 29 October 2018

Accepted 29 October 2018

Available online 31 October 2018

Keywords:

CuS/g-C₃N₄ composites

Fenton-like catalysis

Photocatalysis

Round-the-clock photocatalyst

ABSTRACT

Organic pollutants in industrial and agricultural sewage are a serious threat to the environment and human health. Achieving continuous photocatalytic degradation of organic pollutants under light and dark conditions would have exciting implications for practical sewage treatment. In this paper, CuS/g-C₃N₄ composite catalysts with CuS nanoparticles anchored on g-C₃N₄ sheets were successfully fabricated via a simple solvothermal reaction. The morphology, structure, optical absorption characteristics, electron-hole recombination rate, and degradation performance of the as-prepared CuS/g-C₃N₄ catalysts were investigated in detail. The results confirmed that the as-fabricated CuS/g-C₃N₄ catalysts exhibited high Fenton-like catalytic degradation efficiencies in the dark, and rapid concerted Fenton-like catalytic, direct H₂O₂ photocatalytic and CuS/g-C₃N₄ photocatalytic degradation activities under visible light. Thus, the as-fabricated CuS/g-C₃N₄ catalysts can degrade organic pollutants continuously during both day and night. These degradation properties, along with the simple catalyst fabrication process, will facilitate the practical application of this system in the continuous removal of organic pollutants.

© 2018 The Authors. Published by Elsevier B.V. on behalf of Cairo University. This is an open access article under the CC BY-NC-ND license (<http://creativecommons.org/licenses/by-nc-nd/4.0/>).

Introduction

Sewage purification, especially the removal of organic molecular pollutants including dyes, pesticides, and plasticizers, has gained considerable attention owing to its great importance for ecological and human health [1]. To date, various methods, including adsorption [2–4], filtration [5], biodegradation [6], chemical catalysis [7]

and photocatalysis [8,9], have been successfully developed for the removal of these organic pollutants. Among these methods, photocatalytic degradation has emerged as one of the most promising technologies because it is typically inexpensive and environmentally friendly, readily uses solar light, and does not generate secondary pollutants [8–10]. However, common photocatalysts, such as TiO₂, ZnO, Fe₂O₃, SrTiO₃, or other oxide-based species, show low or no catalytic activity in the absence of light, which greatly hinders their practical applicability for the continuous, around-the-clock degradation of organic pollutants [8–13]. Therefore, developing novel photocatalysts that are highly efficient in the absence of

Peer review under responsibility of Cairo University.

* Corresponding authors.

E-mail addresses: wyun1989@126.com (Y. Wang), sun1th@163.com (T. Sun).<https://doi.org/10.1016/j.jare.2018.10.003>

2090-1232/© 2018 The Authors. Published by Elsevier B.V. on behalf of Cairo University.

This is an open access article under the CC BY-NC-ND license (<http://creativecommons.org/licenses/by-nc-nd/4.0/>).

light is a high priority, and would have great significance for achieving continuous catalytic degradation of organic pollutants.

Graphitic carbon nitride ($g\text{-C}_3\text{N}_4$) is a promising visible-light-driven photocatalyst with a narrow band gap of approximately 2.70 eV [14]. This material is composed of earth abundant elements and can be easily prepared by pyrolysis of nitrogen-rich precursors. However, because of fast charge recombination, the photocatalytic performance of $g\text{-C}_3\text{N}_4$ remains limited by its low efficiency. To improve the photocatalytic performance of $g\text{-C}_3\text{N}_4$, various strategies, such as metal/non-metal doping, noble metal deposition, or compositing with heterogeneous semiconductors [15,16], have been developed. These strategies readily promote charge separation and enhance photocatalytic activity. However, endowing the resultant $g\text{-C}_3\text{N}_4$ -based photocatalysts with highly efficient catalytic activity without light is still challenging.

Copper sulfide (CuS) has been proven to be a suitable semiconductor for use in composites with $g\text{-C}_3\text{N}_4$ to obtain catalysts with enhanced photocatalytic activity [17,18]. For example, Yu et al. integrated $g\text{-C}_3\text{N}_4$ nanosheets with hexagonal CuS nanoplates to synthesize a $g\text{-C}_3\text{N}_4\text{-CuS}$ nanocomposite photocatalyst and demonstrated that the prepared $g\text{-C}_3\text{N}_4\text{-CuS}$ had a much higher hydrogen evolution rate ($126.5 \mu\text{mol}\cdot\text{h}^{-1}$) than a pure $g\text{-C}_3\text{N}_4$ nanosheet under solar light [17]. Chen et al. also reported that a porous $g\text{-C}_3\text{N}_4/\text{CuS}$ heterostructured photocatalyst exhibited enhanced photocatalytic performance towards the degradation of various organic dyes under visible light irradiation [18]. Note that CuS is not only a good co-photocatalyst, but also a Fenton-like catalyst, a type of catalyst that can effectively degrade a wide range of organic pollutants with the help of hydrogen peroxide (H_2O_2) with or without light [19,20]. The Fenton reaction is a catalytic process that generates hydroxyl radicals from H_2O_2 , and the hydroxyl radical is a powerful oxidant that can oxidize organic molecules into lower-molecular-weight molecules or carbon dioxide and water [21]. Therefore, a composite of CuS and $g\text{-C}_3\text{N}_4$ may exhibit both enhanced photocatalytic activity and Fenton-like catalytic activity, and provide an alternative method for achieving continuous degradation of organic pollutants both with and without light.

In this study, $\text{CuS}/g\text{-C}_3\text{N}_4$ composite catalysts were fabricated and used to treat dye-containing sewage in the dark and under visible light irradiation to verify the above speculations. UV-vis and photoluminescence (PL) spectra showed broad visible light absorption and a low photoinduced carrier recombination rate. When used to degrade a dye-containing solution with the help of H_2O_2 , the $\text{CuS}/g\text{-C}_3\text{N}_4$ catalysts exhibited high Fenton-like catalytic activity in the degradation of rhodamine B [RhB, 30 mg mL^{-1}] in the dark and excellent photocatalytic and Fenton-like catalytic activity under visible light. Moreover, the as-fabricated $\text{CuS}/g\text{-C}_3\text{N}_4$ may be a promising catalyst for achieving continuous catalytic activity in highly concentrated dye wastewaters, which would be of great use in practical applications.

Experimental

Materials

Melamine, copper (II) chloride dihydrate ($\text{CuCl}_2\cdot 2\text{H}_2\text{O}$), sodium dodecyl benzene sulfonate (SDBS), thioacetamide (TAA), anhydrous ethanol, ethylene glycol and RhB of analytical-reagent grade were purchased from Sinopharm Chemical Reagent Co., Ltd., Shanghai, China. All reagents were used as received.

Fabrication of the $\text{CuS}/g\text{-C}_3\text{N}_4$ catalysts

The fabrication of the $\text{CuS}/g\text{-C}_3\text{N}_4$ catalysts is schematically illustrated in Fig. S1. Bulk $g\text{-C}_3\text{N}_4$ was fabricated by direct heating of melamine at 550°C in air for 5 h at a heating rate of $5^\circ\text{C}\cdot\text{min}^{-1}$

from room temperature. CuS powder was prepared as follows: 0.341 g of $\text{CuCl}_2\cdot 2\text{H}_2\text{O}$ and 0.025 g of SDBS were dissolved in 100 mL of deionized water. TAA (50 mL, 0.12 M) was added to the above solution. Then, the flask containing the solution was immersed in a constant temperature bath (100°C) for 4 h. The dark product was washed repeatedly with ethanol and deionized water, and then oven-dried at 50°C for 12 h.

The $\text{CuS}/g\text{-C}_3\text{N}_4$ catalysts were fabricated using a simple solvothermal reaction. Typically, 0.5 g of $g\text{-C}_3\text{N}_4$ and 0.03 g of CuS were dispersed in 25 mL of glycol. After ultrasonic treatment for 30 min, the solution was stirred for 1 h to thoroughly mix the components. Then, the solution was sealed in a polytetrafluoroethylene (Teflon)-lined stainless-steel autoclave, and heated to 190°C for 24 h. The product was washed repeatedly with ethanol and deionized water, and the $\text{CuS}/g\text{-C}_3\text{N}_4$ catalyst was collected. The same process was applied to obtain the other $\text{CuS}/g\text{-C}_3\text{N}_4$ catalysts with different CuS contents. The resultant $\text{CuS}/g\text{-C}_3\text{N}_4$ catalysts were labelled $x\%\text{-CuS}/g\text{-C}_3\text{N}_4$, where x is the weight ratio of CuS to $g\text{-C}_3\text{N}_4$. In this work, catalysts with x values of 0, 2, 4, 6, 8, and 10 were prepared.

Characterization

The crystal structures of the samples were evaluated using a Rigaku D/MAX 2550 X-ray diffractometer with $\text{Cu K}\alpha$ radiation (50 kV, 200 mA) (Rigaku Co., Tokyo, Japan). The morphology and elemental composition of each sample was determined using field-emission scanning electron microscopy (FESEM, JEOL JSM 6700F, Japan) and transmission electron microscopy (TEM, FEI Tecnai G2S-Twin, America). UV-vis diffuse reflectance spectroscopy (DRS) was performed using a SHIMADZU 2550 UV/vis spectrophotometer (Japan). The PL spectra of the photocatalysts were acquired on a fluorescence spectrophotometer (Fluoromax-4 HORIBA Jobin Yvon, America). The UV-vis spectra of the dye suspensions were obtained on a UV-vis spectrometer (TU-1901, Persee, Beijing, China).

Catalytic activity

To assess the catalytic ability of the $\text{CuS}/g\text{-C}_3\text{N}_4$ catalysts, a RhB solution was catalytically degraded at room temperature in the dark and under visible light (300 W Xe lamp, $\lambda \geq 420 \text{ nm}$). Typically, 40 mg of the $\text{CuS}/g\text{-C}_3\text{N}_4$ catalyst was added to 100 mL of a $30 \text{ mg}\cdot\text{L}^{-1}$ RhB solution, and the suspension was stirred in the dark for 30 min to establish the adsorption-desorption equilibrium between RhB and the $\text{CuS}/g\text{-C}_3\text{N}_4$ catalyst. Then, 0.5 mL of 30% hydrogen peroxide (H_2O_2) was added to initiate the reaction both in the dark and under visible light. The concentration of the suspension was analysed every 10 min by a UV-vis spectrophotometer. The reproducibility of the results was evaluated by repeating the experiments at least three times, first for 30 min in the dark, and then for 30 min under visible light. The same test procedures were applied to all control experiments and experiments using different amounts of H_2O_2 or different amounts of $6\%\text{-CuS}/g\text{-C}_3\text{N}_4$. Considering the major role of CuS in the Fenton degradation reaction in the dark, we performed a comparative experiment with the same content of CuS, namely, 40 mg of $6\%\text{-CuS}/g\text{-C}_3\text{N}_4$ and 2.4 mg of pure CuS, to compare the Fenton catalytic capacities of pure CuS and $6\%\text{-CuS}/g\text{-C}_3\text{N}_4$ in the dark.

To verify the continuous catalytic activity of the $\text{CuS}/g\text{-C}_3\text{N}_4$ catalysts in highly concentrated dye wastewater in the absence and presence of light, 40 mg of the $6\%\text{-CuS}/g\text{-C}_3\text{N}_4$ catalyst was added to 150 mL of a $150 \text{ mg}\cdot\text{L}^{-1}$ RhB solution, and the solution was stirred in the dark for 30 min. Then, 0.5 mL of H_2O_2 was added to initiate the reaction, and the solution was held in the dark for 1 h. The reaction was then continued under visible light for an additional

1 h. The concentration of the suspension was analysed every 20 min. Then, 0.5 mL of H₂O₂ was added to the remaining suspension to restart the reaction cycle. This reaction process was maintained for three cycles.

Results and discussion

Characteristics of the CuS/g-C₃N₄ catalysts

The CuS/g-C₃N₄ catalysts were fabricated by a simple solvothermal reaction of bulk g-C₃N₄ and CuS powder. Fig. 1 shows the X-ray diffraction (XRD) patterns of pure CuS, pure g-C₃N₄ and the x%-CuS/g-C₃N₄ composites, where x is the weight ratio of CuS to g-C₃N₄. Two main peaks appear for pure g-C₃N₄ and all the CuS/g-C₃N₄ composites. The distinct peaks at 13.1° and 27.4° can be readily indexed as the (1 0 0) and (0 0 2) crystal planes of g-C₃N₄, respectively [JCPDS, no. 87–1526] [22,23]. In addition, there are several small peaks at 29.2°, 31.7°, 32.7°, 47.9°, 52.8° and 59.4° for the CuS/g-C₃N₄ composites, which are consistent with those of pure CuS and can be indexed as the (1 0 2), (1 0 3), (1 0 6), (1 1 0), (1 0 8), and (1 1 6) crystal planes of CuS [JCPDS, no. 06-0464] [19,20]. With increasing CuS content, the diffraction peaks of CuS become more intense.

The structures of the bulk g-C₃N₄, CuS powder and the as-fabricated CuS/g-C₃N₄ catalysts are presented in Fig. 2. The CuS powder is a flower-like aggregate composed of two-dimensional nanoplates (Fig. 2a). The bulk g-C₃N₄ is a wrinkled sheet with a smooth surface. After the solvothermal reaction, the CuS/g-C₃N₄ catalysts took on a sheet-like morphology with anchored nanoparticles. Taking 6%-CuS/g-C₃N₄ as an example, the sheet-like catalyst is rough, and CuS nanoparticles decorate the surface (Fig. 2c and d). The atomic force microscopy (AFM) image in Fig. S2 shows that the 6%-CuS/g-C₃N₄ sheet is approximately 40–50 nm thick. Notably, the as-fabricated 6%-CuS/g-C₃N₄ catalysts are partially aggregated, so the thickness may be greater than what was observed here. The TEM image in Fig. 2e further demonstrates that the CuS nanoparticles are anchored to the g-C₃N₄ sheets. Interestingly, the flower-like CuS particles can be transformed into CuS nanoparticles during the solvothermal reaction, which may enhance the interface between the CuS nanoparticles and the g-C₃N₄ sheets. The high-resolution TEM (HRTEM) image in Fig. 2f clearly shows that fringes

with a lattice spacing of approximately 0.305 nm can be found, and this spacing corresponds to the (1 0 2) plane of CuS [24]. The energy-dispersive X-ray spectroscopy (EDS) elemental analysis data shown in Fig. 2g and h and the elemental mapping images in Fig. S3 further confirm the presence of C, N, Cu and S in the obtained CuS/g-C₃N₄ catalyst, reaffirming the co-existence of CuS and g-C₃N₄.

The nitrogen adsorption–desorption isotherms and the Barrett–Joyner–Halenda pore size distribution curve of 6%-CuS/g-C₃N₄ are displayed in Fig. 3. The adsorption–desorption isotherms are of type IV with a type H3 hysteresis loop, suggesting the formation of slit-shaped mesopores arising from the aggregation of plate-like particles in 6%-CuS/g-C₃N₄. This result is in close agreement with the SEM and TEM observations, which showed 6%-CuS/g-C₃N₄ took on a sheet-like morphology. The pore size distribution of 6%-CuS/g-C₃N₄ confirms that there are hierarchical mesopores with diameters of 3.2, 5.7 and 12.6 nm in the samples. These mesopores may be formed between packed layers. The Brunauer–Emmett–Teller (BET) specific surface areas of 2%-CuS/g-C₃N₄, 4%-CuS/g-C₃N₄, 6%-CuS/g-C₃N₄, 8%-CuS/g-C₃N₄ and 10%-CuS/g-C₃N₄ were calculated to be 114.1, 109.5, 105.4, 87.0 and 66.5 m²·g⁻¹, respectively (Table S1). The total pore volume also decreases from 0.32 to 0.22 cm³·g⁻¹ with increasing CuS content, indicating that compositing CuS with g-C₃N₄ could reduce the specific surface area of x%-CuS/g-C₃N₄. Notably, the BET surface area of pure g-C₃N₄ was calculated to be only 10.3 m²·g⁻¹. The increased BET surface areas of x%-CuS/g-C₃N₄ suggest that the melamine-derived bulk g-C₃N₄ was exfoliated into thin-layered g-C₃N₄ during the solvothermal process, generating a higher BET surface area and more mesopores [18,25,26]. In addition, CuS nanoparticles were anchored on the exfoliated g-C₃N₄ sheets during the solvothermal process, which may improve the dispersion of CuS nanoparticles and enhance the interface between the CuS nanoparticles and the g-C₃N₄ sheets. Higher BET specific surface areas and more mesopores can improve the adsorption rate and adsorption capacity of a catalyst and provide more active sites, leading to higher catalytic capacities. Thus, it can be inferred that the catalytic capacity of the CuS/g-C₃N₄ composites is determined not only by their CuS content but also by their BET surface area and pore volume.

The optical absorption characteristics and electron–hole recombination rate of the as-prepared CuS, g-C₃N₄ and CuS/g-C₃N₄ catalysts were studied by UV–vis DRS and PL spectroscopy, respectively. As shown in Fig. 4a, pure g-C₃N₄ shows a fundamental absorption edge at approximately 455 nm in the visible light region. The corresponding band gap energy (E_g) was calculated to be 2.73 eV ($E_g = 1240/\lambda$, λ is the absorption wavelength), which is very close to the reported value for g-C₃N₄ nanosheets [27]. Pure CuS has a wide absorption range of 300 to 800 nm, which is in good agreement with its intrinsic green-black colour. The absorption edge of pure CuS is at approximately 900 nm, and the corresponding band gap energy is 1.38 eV. In addition, the potentials of the valance band (E_{VB}) and conduction band (E_{CB}) of a semiconductor can be calculated via the following empirical equations [18]:

$$E_{VB} = X_{\text{semiconductor}} - E^\circ + 0.5E_g \quad (1)$$

$$E_{CB} = E_{VB} - E_g \quad (2)$$

where $X_{\text{semiconductor}}$ is the electronegativity of the semiconductor, and E° is the energy of free electrons vs. hydrogen (approximately 4.5 eV/NHE). The $X_{\text{semiconductor}}$ values of g-C₃N₄ and CuS are 4.64 eV and 5.27 eV, respectively. The band gap energies (E_g values) of g-C₃N₄ and CuS were estimated at 2.73 eV and 1.38 eV, respectively. The E_{VB} and E_{CB} potentials of g-C₃N₄ and CuS could be calculated to be 1.51 eV/NHE and –1.22 eV/NHE and 0.83 eV/NHE and –0.55 eV/NHE, respectively.

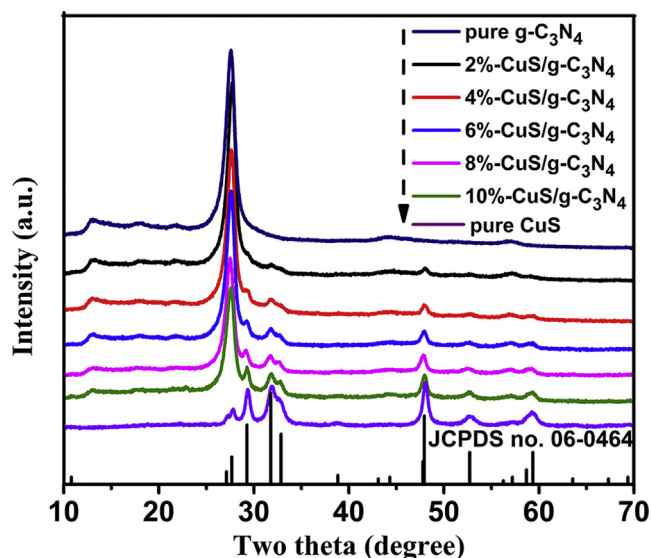


Fig. 1. XRD patterns of pure CuS, pure g-C₃N₄ and x%-CuS/g-C₃N₄ composites, where x is the weight ratio of CuS to g-C₃N₄.

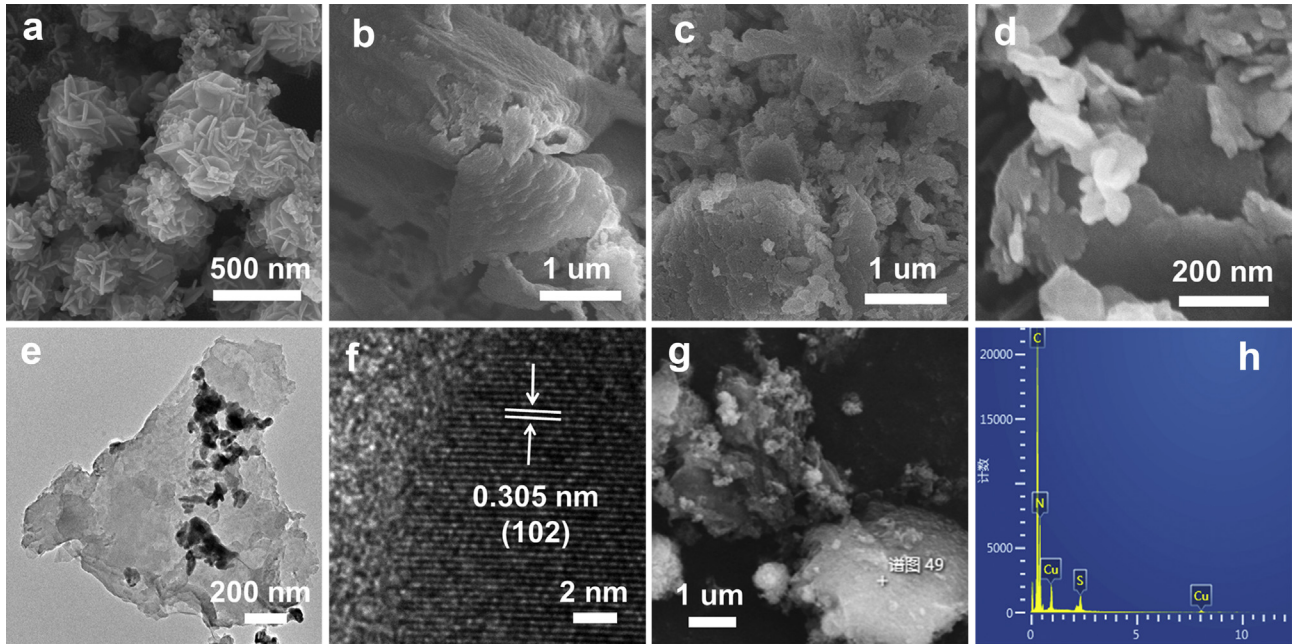


Fig. 2. (a) SEM image of pure CuS; (b) SEM image of pure g-C₃N₄; (c) SEM, (d) high-magnification SEM, (e) TEM, and (f) HRTEM images of 6%-CuS/g-C₃N₄; (g) and (h) EDS elemental analysis of 6%-CuS/g-C₃N₄.

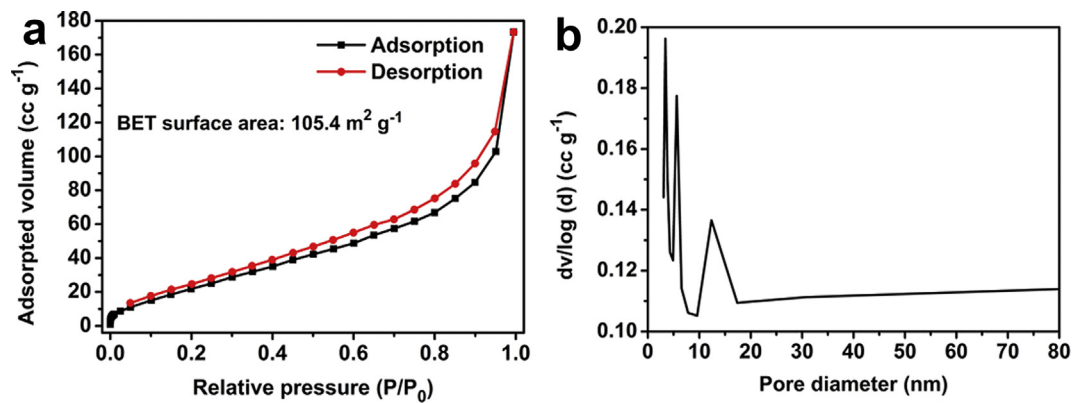


Fig. 3. (a) N₂ adsorption-desorption isotherms and (b) the corresponding pore-size distribution curve of 6%-CuS/g-C₃N₄.

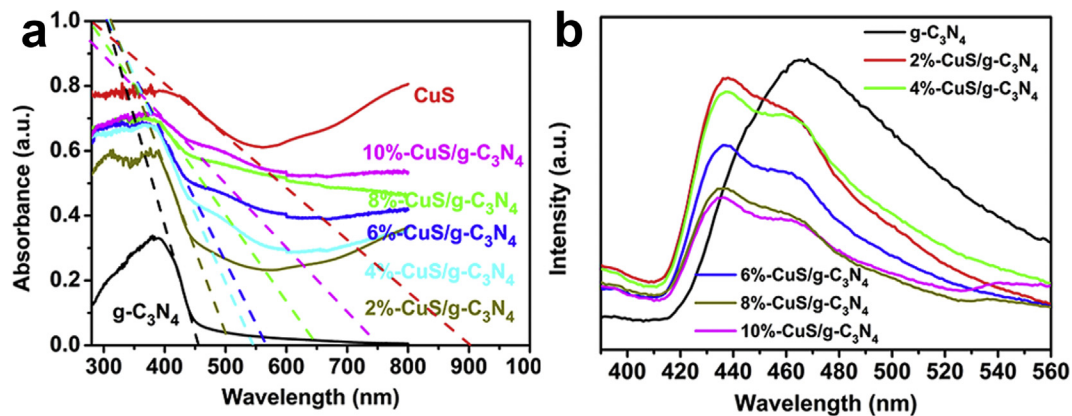


Fig. 4. (a) UV-vis absorption spectra of g-C₃N₄, CuS and x%-CuS/g-C₃N₄ catalysts and (b) PL spectra of g-C₃N₄ and x%-CuS/g-C₃N₄ catalysts.

When CuS is added, the resulting x%-CuS/g-C₃N₄ composites show better visible light absorption. The absorption edges of 2%-CuS/g-C₃N₄, 4%-CuS/g-C₃N₄, 6%-CuS/g-C₃N₄, 8%-CuS/g-C₃N₄, and

10%-CuS/g-C₃N₄ had shifted to 506, 546, 569, 650 and 753 nm, and the corresponding band gap energies were 2.45, 2.27, 2.18, 1.91 and 1.65 eV, respectively. Smaller band gaps mean the less

energy is required to induce efficient electron transfer. Moreover, the electron–hole recombination rates of the as-prepared $g\text{-C}_3\text{N}_4$ and $\text{CuS}/g\text{-C}_3\text{N}_4$ catalysts were investigated by PL spectroscopy (Fig. 4b). The PL peaks of $x\%\text{-CuS}/g\text{-C}_3\text{N}_4$ were blueshifted relative to that of bulk $g\text{-C}_3\text{N}_4$. The blueshift can presumably be attributed to the decrease in the conjugation length and the strong quantum confinement effect due to the few-layer structure of the $g\text{-C}_3\text{N}_4$ nanosheets. This result further verified that the melamine-derived bulk $g\text{-C}_3\text{N}_4$ was exfoliated into thin-layered $g\text{-C}_3\text{N}_4$ during the solvothermal process. Similar observations have been reported in other studies [25,28]. A lower PL peak intensity indicates a lower electron–hole recombination rate and a higher electron-transfer rate [17]. The as-obtained $x\%\text{-CuS}/g\text{-C}_3\text{N}_4$ composites show lower peak intensities than pure $g\text{-C}_3\text{N}_4$, suggesting that the CuS nanoparticles anchored on the surface of $g\text{-C}_3\text{N}_4$ could efficiently transfer the electrons generated from $g\text{-C}_3\text{N}_4$ [16]. A lower electron–hole recombination rate can be achieved by increasing the CuS content. Therefore, the good suppression of recombination and good visible light absorption of $x\%\text{-CuS}/g\text{-C}_3\text{N}_4$, as well as the high BET specific surface area, would contribute to their better photocatalytic activity towards organic pollutants in sewage under visible light. With the addition of the Fenton-like catalytic activities of CuS [19,20], the as-obtained $\text{CuS}/g\text{-C}_3\text{N}_4$ catalysts were expected to achieve continuous degradation of organic pollutants both with and without light.

Degradation performance of the $\text{CuS}/g\text{-C}_3\text{N}_4$ catalysts

The degradation performance of the $\text{CuS}/g\text{-C}_3\text{N}_4$ catalysts towards organic pollutants was evaluated by decomposing RhB with the help of H_2O_2 in the dark and under visible light. First, the degradation behaviors of $x\%\text{-CuS}/g\text{-C}_3\text{N}_4$ composites were investigated under visible light. As shown in Fig. 5a, the time profiles of C/C_0 , where C_0 and C represent the initial and reaction concentrations of the RhB solution, respectively, indicate that for all samples, the $\text{CuS}/g\text{-C}_3\text{N}_4$ catalysts exhibited higher degradation activity than pure CuS and $g\text{-C}_3\text{N}_4$, which confirms that the interface between CuS and $g\text{-C}_3\text{N}_4$ could successfully suppress electron–hole recombination and improve the photocatalytic activity. Among the catalysts, 6%– $\text{CuS}/g\text{-C}_3\text{N}_4$ shows the best degradation performance; it degraded approximately 95% of the RhB in 60 min. The corresponding degradation rate constants (k) were calculated assuming a pseudo-first-order reaction based on $\ln(C_0/C) = kt$ (Fig. 5b). The rate constant with 6%– $\text{CuS}/g\text{-C}_3\text{N}_4$ is 0.04924 min^{-1} , which is greater than that of each of the other catalysts. These results confirm that there is an optimal content of CuS in the composite, which in this work is 6%, that provides the best

degradation performance. Thus, the following discussion will focus on the 6%– $\text{CuS}/g\text{-C}_3\text{N}_4$ catalyst.

The effects of the amounts of H_2O_2 and the catalyst (6%– $\text{CuS}/g\text{-C}_3\text{N}_4$) on the catalytic degradation of RhB under visible light were also investigated. As shown in Fig. 6a and b, when the amount of H_2O_2 was varied from 0.1 to 0.5 mL, the RhB degradation efficiency increases rapidly from 55% to 95%, but when the amount is increased further (to 0.9 mL), the efficiency remains almost unchanged. This phenomenon is similar to what is seen in other organic pollutant degradation systems under light [29,30]. At low H_2O_2 concentrations, the improvement in efficiency is mainly due to the $\cdot\text{OH}$ radicals generated from H_2O_2 under light irradiation and the fact that H_2O_2 is a good electron acceptor [31,32]. At high H_2O_2 concentrations, the excess H_2O_2 molecules scavenge the valuable $\cdot\text{OH}$ species, leading to a slight decrease in the efficiency [33]. Thus, the optimal amount of H_2O_2 for the catalytic degradation of RhB under visible light is 0.5 mL. The relationship between the degradation efficiency and the amount of 6%– $\text{CuS}/g\text{-C}_3\text{N}_4$ catalyst is shown in Fig. 6c and d. In 60 min, the degradation efficiency increases rapidly from 55% to 95% when the amount of catalyst is increased from 20 to 40 mg, and the efficiency decreases slightly (to 89%) when the amount of catalyst is increased further to 60 mg. It is generally accepted that increasing the catalyst loading would increase the light absorption and pollutant adsorption, leading to improved catalytic activity. However, a further increase in the catalyst loading may cause light scattering and screening effects, which would reduce the specific activity [34,35]. In addition, aggregation of the catalyst may also reduce the catalytic activity [35]. Thus, in this work, the optimal amount of the 6%– $\text{CuS}/g\text{-C}_3\text{N}_4$ catalyst to achieve the best degradation performance was found to be 40 mg.

To further understand the catalytic mechanism of the 6%– $\text{CuS}/g\text{-C}_3\text{N}_4$ catalyst and the potential for around-the-clock catalytic activity, comparative experiments on the degradation of RhB in the dark were conducted. Considering the major role of CuS in the Fenton degradation reaction in the dark, we performed a comparative experiment using the same CuS content, namely, 40 mg of 6%– $\text{CuS}/g\text{-C}_3\text{N}_4$ compared with 2.4 mg of pure CuS. As shown in Fig. 7a, the 6%– $\text{CuS}/g\text{-C}_3\text{N}_4$ catalyst shows high catalytic efficiency in decomposing RhB with the help of H_2O_2 in the dark. The catalyst can degrade approximately 74% of the RhB in 60 min. Pure $g\text{-C}_3\text{N}_4$ shows no catalytic activity, and pure CuS degrades approximately 46% of the RhB in 60 min. CuS catalysts have been demonstrated to be highly efficient Fenton-like reagents [19,20]. $\text{OH}\cdot$ was generated from the degradation of H_2O_2 in the presence of a CuS catalyst, and the highly reactive $\text{OH}\cdot$ could oxidize the organic pollutant (RhB) into smaller molecules (CO_2 , H_2O , etc.). The 6%– $\text{CuS}/g\text{-C}_3\text{N}_4$

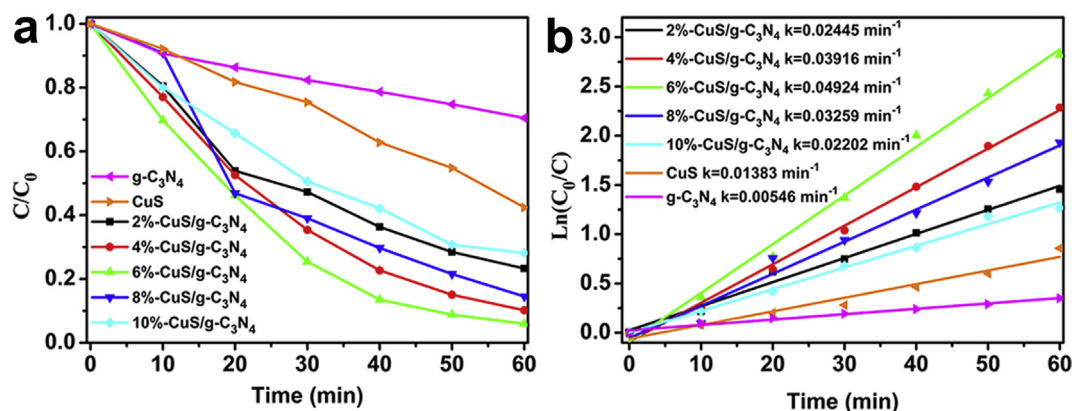


Fig. 5. (a) The degradation of RhB monitored at normalized concentration change (C/C_0) vs. irradiation time (t) and (b) reaction rate constants associated with RhB degradation.

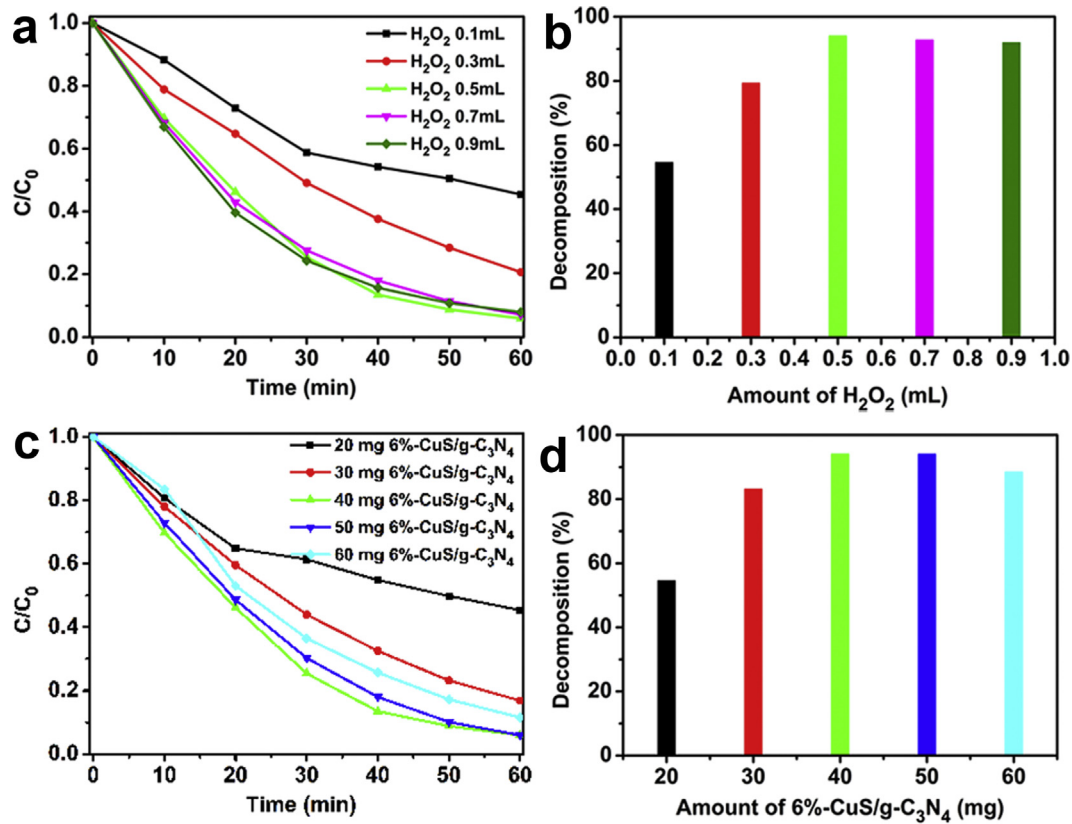
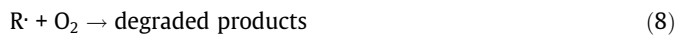
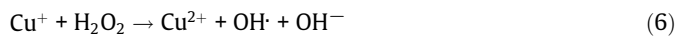


Fig. 6. (a) Degradation and (b) degradation efficiency of RhB with different amounts of H_2O_2 ; (c) degradation, and (d) degradation efficiency of RhB with different amounts of 6%-CuS/g- C_3N_4 .

catalyst may promote similar Fenton-like degradation reactions in the current work, and the improved catalytic activity may be due to the good dispersion of CuS nanoparticles anchored on the $\text{g-C}_3\text{N}_4$ nanosheets and the interface between the CuS nanoparticles and $\text{g-C}_3\text{N}_4$ sheets. Accordingly, the Fenton-like reaction mechanism can be described as follows [19,20]:

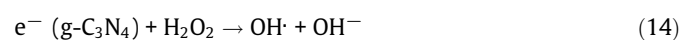
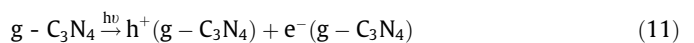


In the absence of H_2O_2 , the 6%-CuS/g- C_3N_4 catalyst shows no catalytic activity. Thus, in this work, the addition of H_2O_2 is regarded as the start of the degradation reaction. Furthermore, H_2O_2 alone, in the absence of the catalyst, cannot degrade the RhB solution in the dark (Fig. 7b). Photolysis of H_2O_2 can slowly produce reactive $\text{OH}\cdot$, leading to a low degradation efficiency of 5% in 60 min under visible light [36].



Thus, three degradation pathways exist under visible light, namely, the Fenton-like degradation reaction, the direct H_2O_2 photocatalytic degradation reaction and the CuS/g- C_3N_4 photocatalytic degradation reaction.

Studies have shown that CuS/g- C_3N_4 composites are efficient photocatalysts for pollutant degradation and water splitting [17,18]. Under visible light, both CuS and $\text{g-C}_3\text{N}_4$ could photoinduce electron-hole pairs [Eqs. (10) and (11)]. The conduction band (CB)/valence band (VB) potentials of CuS and $\text{g-C}_3\text{N}_4$ are $-0.55/+0.83$ and $-1.22/+1.51$ eV, respectively. The CB of $\text{g-C}_3\text{N}_4$ is more negative than that of CuS, so the photoinduced electrons [$e^-(\text{g-C}_3\text{N}_4)$] in the CB of $\text{g-C}_3\text{N}_4$ could easily transfer to the CB of CuS. Due to the standard reduction potentials of -0.33 eV/NHE (O_2/O_2^-) and 0.32 eV/NHE ($\text{H}_2\text{O}_2/\text{OH}\cdot, \text{OH}^-$), electrons in the conduction band of CuS (-0.55 eV/NHE) and $\text{g-C}_3\text{N}_4$ (-1.22 eV/NHE) could react with O_2 to form $\cdot\text{O}_2^-$ radicals [Eqs. (12) and (13)] and react with H_2O_2 to form $\text{OH}\cdot$ and OH^- radicals [Eqs. (14) and (15)]. These photogenerated oxidant species ($\text{OH}\cdot$ and $\cdot\text{O}_2^-$) have a high oxidative capacity to degrade organic pollutants [Eq. (16)] [37]. At the same time, the holes in the VB of $\text{g-C}_3\text{N}_4$ and CuS could be directly consumed by reactions with organic pollutants [Eqs. (17) and (18)] [18]. A schematic illustration of the possible photocatalytic mechanism is shown in Fig. 7c.



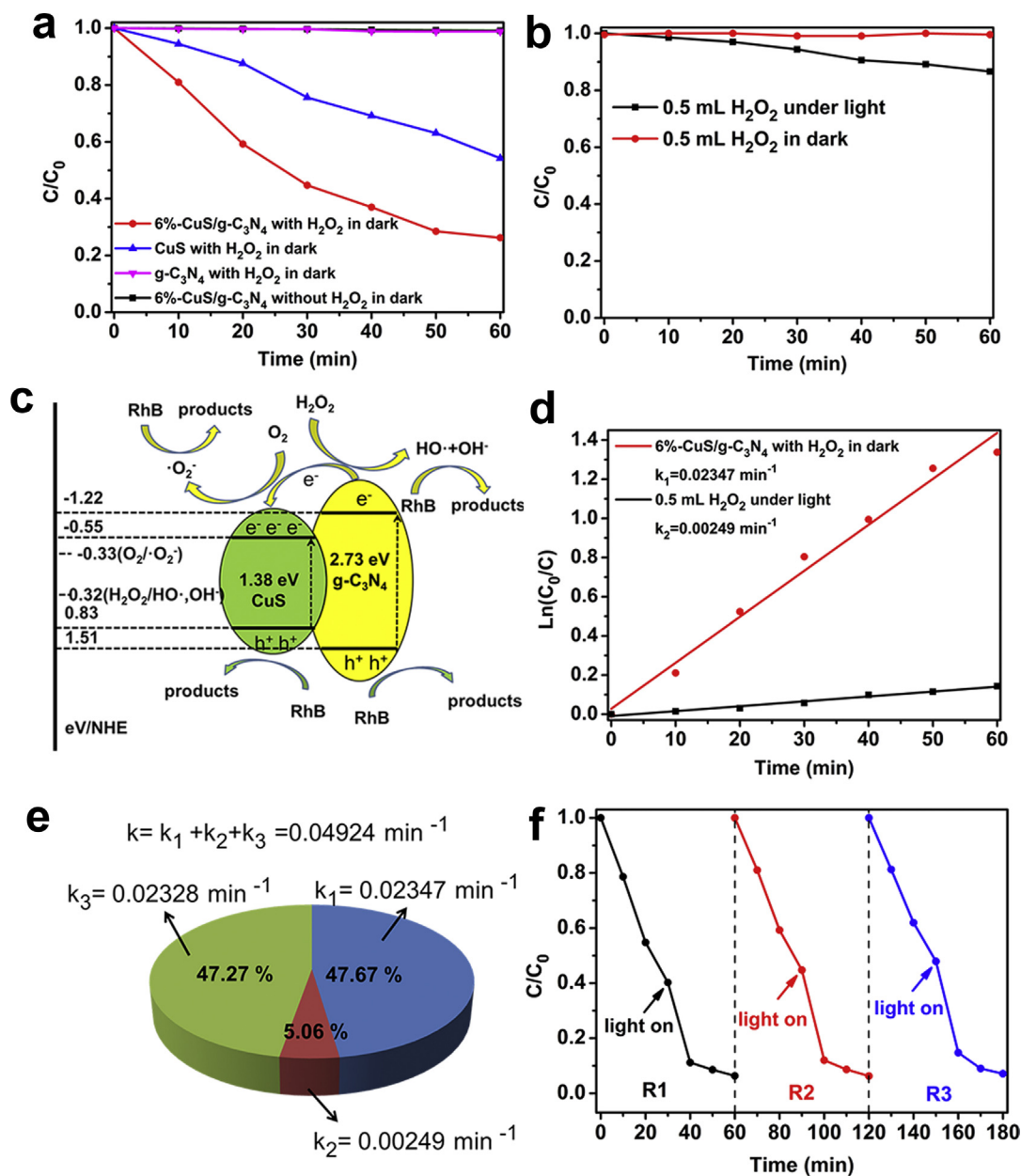
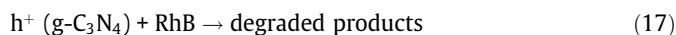
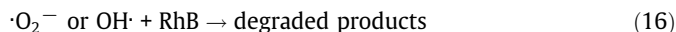


Fig. 7. (a) The degradation of RhB in the dark with different catalysts; (b) the degradation of RhB with H₂O₂ under light or in the dark; (c) a schematic illustration of the possible photocatalytic mechanisms; (d) the reaction rate constants associated with RhB degradation; (e) the proportional distribution of different degradation pathways; and (f) cyclic runs of 6%-CuS/g-C₃N₄ for the degradation of RhB in the dark and under visible light irradiation.



The enhanced CuS/g-C₃N₄ photocatalytic degradation reaction, in combination with the Fenton-like degradation reaction and the direct H₂O₂ photocatalytic degradation reaction, is responsible for the good degradation performance of the CuS/g-C₃N₄ catalysts towards organic pollutants. Notably, these three degradation pathways may have synergistic effects on the degradation of RhB under visible light, further enhancing the photocatalytic activity of this system. Assuming that these reactions occur separately, the Fenton-like reaction of 6%-CuS/g-C₃N₄ with H₂O₂ in the dark can be considered analogous to the Fenton-like reaction under light. Both the Fenton-like degradation reaction and the direct

H₂O₂ photocatalytic degradation reaction can be approximated as pseudo-first-order reactions based on $\ln(C_0/C) = kt$ (Fig. 7d). The rate constants of the Fenton-like reaction and direct H₂O₂ photocatalytic reaction are 0.02347 (k_1) and 0.00249 (k_2) min⁻¹, respectively. The total rate constant is 0.04924 min⁻¹ (k) (Fig. 5b). Thus, the rate constant of the 6%-CuS/g-C₃N₄ photocatalytic degradation reaction can be calculated to be 0.02328 min⁻¹ (k_3). The proportional distribution of the different degradation pathways is shown in the pie chart in Fig. 7e. Thus, the good degradation performance of 6%-CuS/g-C₃N₄ under visible light may arise from the combined advantages of (1) the synergistic effects of the Fenton-like reaction, direct H₂O₂ photocatalytic reaction and CuS/g-C₃N₄ photocatalytic degradation reaction, (2) the enhanced charge separation efficiency caused by the CuS-g-C₃N₄ heterojunction owing to interfacial electron and hole transfer between CuS and g-C₃N₄ and (3) the high BET surface area of 6%-CuS/g-C₃N₄.

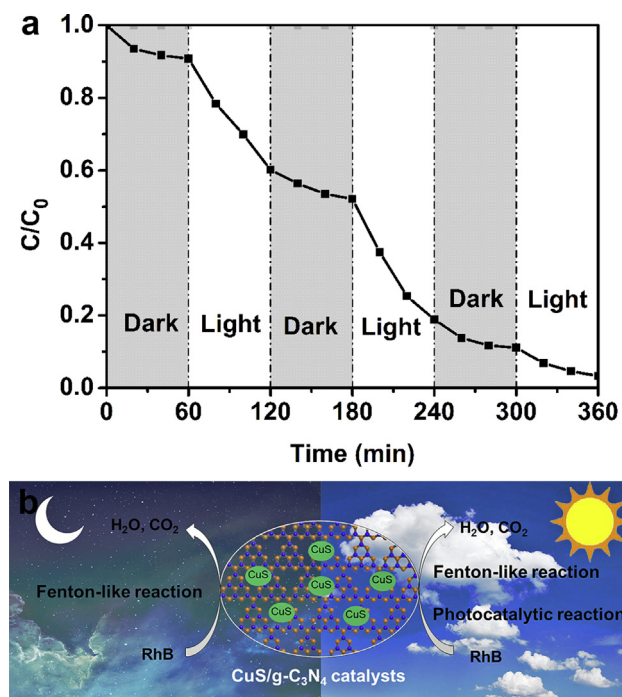


Fig. 8. (a) Continuous degradation of RhB by 6%-CuS/g-C₃N₄ during three dark–light cycles; (b) schematic diagram of the continuous degradation of organic pollutants with the as-fabricated 6%-CuS/g-C₃N₄ catalyst.

The stability of a catalyst is one of the most important indicators of its practical applicability. The stability of the as-fabricated 6%-CuS/g-C₃N₄ was investigated by recycling 6%-CuS/g-C₃N₄ in repeated degradation experiments with and without light, and the results are shown in Fig. 7f. 6%-CuS/g-C₃N₄ maintains a similar level of catalytic activity after three reaction cycles, which indicates that 6%-CuS/g-C₃N₄ has good photochemical stability. Furthermore, SEM images of 6%-CuS/g-C₃N₄ before and after the recycling experiments are shown in Fig. S4. There are no obvious changes after the recycling reaction, which further indicates the high stability of the as-fabricated CuS/g-C₃N₄ catalyst.

Because the as-fabricated CuS/g-C₃N₄ catalysts exhibited high catalytic degradation activity both in the dark and under visible light, CuS/g-C₃N₄ is expected to be a promising catalyst for achieving continuous degradation of organic pollutants in the presence and absence of light. A controlled experiment on degradation of RhB at a high concentration (150 mg·L⁻¹) was conducted in the dark and under visible light to verify the continuous catalytic activity of the 6%-CuS/g-C₃N₄ catalyst. As shown in Fig. 8a, the RhB in the solution was degraded continuously during three dark–light cycles. The catalyst degraded approximately 97% of the RhB in 360 min. In contrast to the reported around-the-clock photocatalysts that can store some photoexcited charge carriers (e⁻/h⁺) while under illumination and release them in the dark to achieve catalytic activity even in the dark [11,38–40], the photocatalysts described in this work demonstrate that combining a Fenton-like reaction and a photocatalytic reaction can also be a promising alternative strategy for designing and constructing new types of continuous photocatalysts for practical applications (Fig. 8b).

Conclusions

CuS/g-C₃N₄ composite catalysts with CuS nanoparticles anchored on g-C₃N₄ sheets were successfully fabricated via a simple solvothermal reaction. UV–vis and PL spectroscopy indicated that the CuS/g-C₃N₄ composites have good visible light absorption

and can efficiently transfer photoinduced electron–hole pairs at the interface between CuS and g-C₃N₄, which can improve its photocatalytic activity towards organic pollutants in sewage under visible light. In addition, the as-fabricated CuS/g-C₃N₄ composites exhibit efficient Fenton-like catalytic activity, and they can degrade organic pollutants in the dark with the help of H₂O₂. Therefore, by combining the enhanced photocatalytic activity and Fenton-like catalytic activity, as well as the direct H₂O₂ photocatalytic reaction, the as-fabricated CuS/g-C₃N₄ composite catalyst system could continuously degrade organic pollutants in the absence and presence of light. Moreover, this finding, which is based on Fenton-like and photocatalytic reactions, may serve as a general strategy for fabricating new types of continuous photocatalysts for practical applications.

Conflicts of interest

The authors have declared no conflict of interest.

Compliance with Ethics Requirements

This article does not describe any studies with human or animal subjects.

Acknowledgements

The authors thank the following funding agencies: the National Natural Science Foundation of China (Nos. 21777021, 21547015 and 21477082), the Fundamental Research Funds for the Central Universities of China (Nos. N162410002-8 and N170504024) and the Doctoral Science Foundation of Liaoning Province (No. 201702280).

Appendix A. Supplementary material

Supplementary data to this article can be found online at <https://doi.org/10.1016/j.jare.2018.10.003>.

References

- [1] Shannon MA, Bohn PW, Elimelech M, Georgiadis JG, Marinakos BJ, Mayes AM. Science and technology for water purification in the coming decades. *Nature* 2008;452:301–10.
- [2] Sui D-P, Chai Y. Removal of bromophenols from aqueous solution by using hazelnut shell-derived activated carbon: equilibrium study and influence of operation conditions. *Chem Lett* 2017;46:516–9.
- [3] Fan H-T, Zhao C-Y, Liu S, Shen H. Adsorption characteristics of chlorophenols from aqueous solution onto graphene. *J Chem Eng Data* 2017;62:1099–105.
- [4] Fan H, Shi LQ, Shen H, Chen X, Xie K-P. Equilibrium, isotherm, kinetic and thermodynamic studies for removal of tetracycline antibiotics by adsorption onto hazelnut shell derived activated carbons from aqueous media. *RSC Adv* 2016;6:109983–91.
- [5] Vandezande P, Gevers LE, Vankelecom IF. Solvent resistant nanofiltration: separating on a molecular level. *Chem Soc Rev* 2008;37:365–405.
- [6] Solís M, Solís A, Pérez HI, Manjarrez N, Flores M. Microbial decolouration of azo dyes: a review. *Process Biochem* 2012;47:1723–48.
- [7] Panizza M, Cerisola G. Electro-Fenton degradation of synthetic dyes. *Water Res* 2009;43:339–44.
- [8] Wang C-C, Li J-R, Lv X-L, Zhang Y-Q, Guo G. Photocatalytic organic pollutants degradation in metal-organic frameworks. *Energy Environ Sci* 2014;7:2831–67.
- [9] Li X, Yu J, Jaroniec M. Hierarchical photocatalysts. *Chem Soc Rev* 2016;45:2603–36.
- [10] Wang Y, Huang H, Gao J, Lu G, Zhao Y, Xu Y, et al. TiO₂-SiO₂ composite fibers with tunable interconnected porous hierarchy fabricated by single-spinneret electrospinning toward enhanced photocatalytic activity. *J Mater Chem A* 2014;2:12442–8.
- [11] Yin H, Chen X, Hou R, Zhu H, Li S, Huo Y, et al. Ag/BiOBr film in a rotating-disk reactor containing long-afterglow phosphor for round-the-clock photocatalysis. *ACS Appl Mater Interfaces* 2015;7:20076–82.
- [12] Sakar M, Nguyen C-C, Vu M-H, Do T-O. Materials and mechanisms of photo-assisted chemical reactions under light and dark conditions: can day-night photocatalysis be achieved? *ChemSusChem* 2018;11:809–20.

- [13] Lu Y, Zhang X, Chu Y, Yu H, Huo M, Qu J, et al. Cu₂O nanocrystals/TiO₂ microspheres film on a rotating disk containing long-afterglow phosphor for enhanced round-the-clock photocatalysis. *Appl Catal B-Environ* 2018;224:239–48.
- [14] Wang Y, Wang X, Antonietti M. Polymeric graphitic carbon nitride as a heterogeneous organocatalyst: from photochemistry to multipurpose catalysis to sustainable chemistry. *Angew Chem Int Ed* 2012;51:68–89.
- [15] Hu S, Ma L, You J, Li F, Fan Z, Lu G, et al. Enhanced visible light photocatalytic performance of g-C₃N₄ photocatalysts co-doped with iron and phosphorus. *Appl Surf Sci* 2014;311:164–71.
- [16] Xu Z, Li H, Wu Z, Sun J, Ying Z, Wu J, et al. Enhanced charge separation of vertically aligned CdS/g-C₃N₄ heterojunction nanocone arrays and corresponding mechanisms. *J Mater Chem C* 2016;4:7501–7.
- [17] Yu S, Webster RD, Zhou Y, Yan X. Ultrathin g-C₃N₄ nanosheets with hexagonal CuS nanoplates as a novel composite photocatalyst under solar light irradiation for H₂ production. *Catal Sci Technol* 2017;7:2050–6.
- [18] Chen X, Li H, Wu Y, Wu H, Wu L, Tan P, et al. Facile fabrication of novel porous graphitic carbon nitride/copper sulfide nanocomposites with enhanced visible light driven photocatalytic performance. *J Colloid Interface Sci* 2016;476:132–43.
- [19] Deng C, Ge X, Hu H, Yao L, Han C, Zhao D. Template-free and green sonochemical synthesis of hierarchically structured CuS hollow microspheres displaying excellent Fenton-like catalytic activities. *CrystEngComm* 2014;16:2738–45.
- [20] Shu QW, Lan J, Gao MX, Wang J, Huang CZ. Controlled synthesis of CuS caved superstructures and their application to the catalysis of organic dye degradation in the absence of light. *CrystEngComm* 2015;17:1374–80.
- [21] Nidheesh PV, Gandhimathi R, Ramesh ST. Degradation of dyes from aqueous solution by Fenton processes: a review. *Environ Sci Pollut Res* 2013;20:2099–132.
- [22] Liao G, Chen S, Quan X, Yu H, Zhao H. Graphene oxide modified g-C₃N₄ hybrid with enhanced photocatalytic capability under visible light irradiation. *J Mater Chem* 2012;22:2721–6.
- [23] Dong F, Zhao Z, Xiong T, Ni Z, Zhang W, Sun Y, et al. In situ construction of g-C₃N₄/g-C₃N₄ metal-free heterojunction for enhanced visible-light photocatalysis. *ACS Appl Mater Interfaces* 2013;5:11392–401.
- [24] Liu J, Xue D. Rapid and scalable route to CuS biosensors: a microwave-assisted Cu-complex transformation into CuS nanotubes for ultrasensitive nonenzymatic glucose sensor. *J Mater Chem* 2011;21:223–8.
- [25] Xu J, Zhang L, Shi R, Zhu Y. Chemical exfoliation of graphitic carbon nitride for efficient heterogeneous photocatalysis. *J Mater Chem A* 2013;1:14766–72.
- [26] Ma F, Sun C, Shao Y, Wu Y, Huang B, Hao X. One-step exfoliation and fluorination of g-C₃N₄ nanosheets with enhanced photocatalytic activities. *New J Chem* 2017;41:3061–7.
- [27] Niu P, Zhang L, Liu G, Cheng H-M. Graphene-like carbon nitride nanosheets for improved photocatalytic activities. *Adv Funct Mater* 2012;22:4763–70.
- [28] Li J, Liu E, Ma Y, Hu X, Wan J, Sun L, et al. Synthesis of MoS₂/g-C₃N₄ nanosheets as 2D heterojunction photocatalysts with enhanced visible light activity. *Appl Surf Sci* 2016;364:694–702.
- [29] Daneshvar N, Salari D, Khataee A. Photocatalytic degradation of azo dye acid red 14 in water: investigation of the effect of operational parameters. *J Photochem Photobiol A* 2003;157:111–6.
- [30] Chu W, Wong CC. The photocatalytic degradation of dicamba in TiO₂ suspensions with the help of hydrogen peroxide by different near UV irradiations. *Water Res* 2004;38:1037–43.
- [31] Hiraoka T, Nosaka Y. Properties of O₂⁻ and OH[•] formed in TiO₂ aqueous suspensions by photocatalytic reaction and the influence of H₂O₂ and some ions. *Langmuir* 2002;18:3247–54.
- [32] Hiraoka T, Yawata K, Nosaka Y. Photocatalytic reactivity for O₂⁻ and OH radical formation in anatase and rutile TiO₂ suspension as the effect of H₂O₂ addition. *Appl Catal A* 2007;325:105–11.
- [33] Muruganandham M, Swaminathan M. Photocatalytic decolourisation and degradation of reactive orange 4 by TiO₂-UV process. *Dyes Pigments* 2006;68:133–42.
- [34] Rahman MA, Muneer M. Photocatalysed degradation of two selected pesticide derivatives, dichlorvos and phosphamidon, in aqueous suspensions of titanium dioxide. *Desalination* 2005;181:161–72.
- [35] Chen S, Liu Y. Study on the photocatalytic degradation of glyphosate by TiO₂ photocatalyst. *Chemosphere* 2007;67:1010–7.
- [36] Barakat MA, Tseng JM, Huang CP. Hydrogen peroxide-assisted photocatalytic oxidation of phenolic compounds. *Appl Catal B* 2005;59:99–104.
- [37] Shi J, Li J, Huang X, Tan Y. Synthesis and enhanced photocatalytic activity of regularly shaped Cu₂O nanowire polyhedra. *Nano Res* 2011;4:448–59.
- [38] Zhou Q, Peng F, Ni Y, Kou J, Lu C, Xu Z. Long afterglow phosphor driven round-the-clock g-C₃N₄ photocatalyst. *J Photochem Photobiol A* 2016;328:182–8.
- [39] Wu H, Peng W, Wang Z-M, Koike K. Cerium-doped gehlenite supporting silver/silver chloride for continuous photocatalysis. *RSC Adv* 2016;6:37995–8003.
- [40] Wu H, Wang Z-M, Koike K, Negishi N, Jin Y. Hybridization of silver orthophosphate with a melilite-type phosphor for enhanced energy-harvesting photocatalysis. *Catal Sci Technol* 2017;17:3736–46.